ChemComm

ROYAL SOCIETY OF CHEMISTRY

COMMUNICATION

View Article Online
View Journal | View Issue

Open Access Article. Published on 29 October 2024. Downloaded on 12/19/2025 2:30:05 PM.
This article is licensed under a Creative Commons Attribution-NonCommercial 3.0 Unported Licence.

Check for updates

Cite this: *Chem. Commun.*, 2024, **60**, 13923

Received 11th July 2024,
Accepted 28th October 2024

DOI: 10.1039/d4cc03468f

rsc.li/chemcomm

Identifying routes for transferring spin polarization from parahydrogen to protic solvents†

Ewoud Vaneeckhaute,*[abc] Jean-Max Tyburn,[d] James G. Kempf,[e] Johan A. Martens[b] and Eric Breynaert*[ab]

Repeatable hyperpolarization of high concentrations of mobile protons (>6 M) using parahydrogen in protic methanol/water mixtures is reported here. Different ammonium buffers with increasing mobile proton concentrations were added to an IrCl(COD)(IMes) catalyst in the presence of pyridine. We reach a maximum molar polarization of 1.79 mM at 6 mT. Field-cycling experiments in an 18.8 T detection field distinguished two solvent polarization transfer pathways: chemical exchange with labile protons from ammonia and cross-relaxation with pyridine aromatic protons.

Parahydrogen induced hyperpolarization (PHIP) techniques have been explored for decades to boost the sensitivity of nuclear magnetic resonance (NMR).[1] Parahydrogen (pH_2), the singlet spin-isomer of molecular H_2, is a portable and cheap source of spin order, allowing high levels of polarization to be produced without requiring large and expensive He-consuming magnets.[2] Generally, pH_2 and target molecules simultaneously coordinate to a transition metal catalyst center (*e.g.* Rh or Ir) at μT to mT magnetic fields. Here, the singlet spin order can become redistributed either by direct hydrogenation or by reversible exchange of the target on the transition metal.[2,3] The latter method is referred to as signal amplification by reversible exchange or SABRE.[4] However, both cases require the use of catalysts, implying chemical specificity, and limiting the substrate scope and application range of PHIP techniques.[5]

In recent years, a multitude of strategies have been proposed to partially circumvent the chemical specificity of PHIP techniques. The strategies range from chemically tailoring targets with suitable functional groups,[6] using co-ligands for regulating the binding characteristics of either too weakly[7] or too strongly ligating targets,[8] or relying on intermediate polarization carrier agents.[9–11] In the latter case, hyperpolarized mobile protons can be used to distribute polarization *via* chemical exchange and subsequent intramolecular polarization transfer (PHIP-X[10] and SABRE-RELAY[9]) or highly polarized molecules transfer polarization to targets directly *via* magnetic exchange caused by dipolar cross-relaxation.[12,13] This is generally referred to as spin polarization induced nuclear Overhauser effect (SPINOE),[14] and has been observed for PHIP when preparing large in-phase polarization using the radiofrequency amplification by stimulated emission of radiation (RASER) technique.[13]

In the liquid state, hyperpolarization of protic solvents can combine the virtues of both chemical and magnetic exchange mechanisms to polarize dissolved molecules.[15] Hyperpolarization techniques based on dissolution dynamic nuclear polarization (dDNP), which uses the high spin polarization of electrons to hyperpolarize nuclear spins, have been the reference solution for hyperpolarizing large molar quantities of protic solvents including water, the ultimate bio-compatible solution.[15] However, dDNP requires complex instrumentation and cryogenic temperatures for best performance and only generates a single shot of the hyperpolarized product.[16]

Parahydrogen-based methods can hyperpolarize protic solvents repeatably and can therefore be a suitable alternative. The generation of hyperpolarized protic solvents including methanol and water by means of pH_2 has been reported before.[17–21] While a diverse range of polarization transfer methods from pH_2 to the solvent were proposed, in each case, only millimolar quantities of labile protons were hyperpolarized since most of the solvent was present in a fully deuterated form. The solvent molar polarization (concentration multiplied by polarization),[11] a quantity that well expresses the polarization efficiency since it

[a] NMRCoRe, NMR/X-Ray Platform for Convergence Research, KU Leuven, Celestijnenlaan 200F, box 2461, B-3001 Leuven, Belgium. E-mail: ewoud.vaneeckhaute@kuleuven.be, eric.breynaert@kuleuven.be
[b] COK-KAT, Centre for Surface Chemistry and Catalysis – Characterisation and Application Team, KU Leuven, Celestijnenlaan 200F, box 2461, B-3001 Leuven, Belgium
[c] Université Claude Bernard Lyon 1, CNRS, ENS Lyon, UCBL, CRMN UMR 5082, 69100 Villeurbanne, France
[d] Bruker Biospin, 34 Rue de l'Industrie BP 10002, 67166 Wissembourg Cedex, France
[e] Bruker Biospin, 15 Fortune Dr, Billerica, 01821 Massachusetts, USA

† Electronic supplementary information (ESI) available: Hardware specifications, experimental methods, SABRE catalyst elucidation, polarization transfer field profile and lifetime analysis. See DOI: https://doi.org/10.1039/d4cc03468f

Open Access Article. Published on 29 October 2024. Downloaded on 12/19/2025 2:30:05 PM.
This article is licensed under a Creative Commons Attribution-NonCommercial 3.0 Unported Licence.

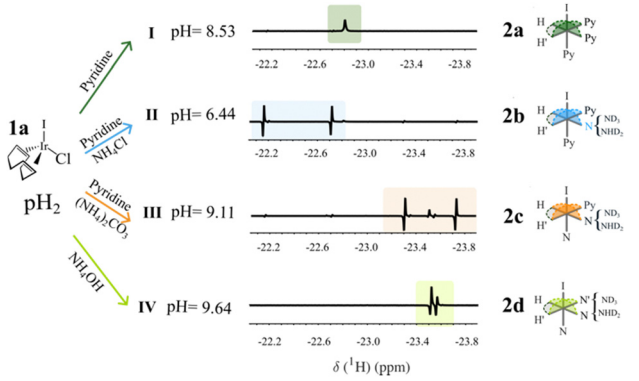

Fig. 1 SABRE mixtures **I–IV** in presence of pH_2, IrCl(COD)(IMes) (**1a**), pyridine (Py) and ammonia (N). The hydride signals measured at 18.8 T after field-cycling were used to determine the dominant SABRE catalysts represented by **2a**, **2b**, **2c** and **2d** depending on the ammonium buffers NH_4Cl, $(NH_4)_2CO_3$ and NH_4OH used. More information on the catalyst elucidation can be found in Fig. S3–S5 of the ESI.†

is proportional to the NMR signal, therefore remains low. Yet to accomplish polarization transfer to targets *via* the protic solvent, high molar polarization levels are required to counter spin-dilution.[22] Until now, dry aprotic solvents such as dichloromethane, acetone, or chloroform were used to limit the quantity of available labile protons sites and to slow down exchange dynamics.[10,11] However, many organic targets cannot be dissolved in aprotic media which limits the future applicability of the method.

Here we report on the repeatable hyperpolarization of high concentrations of mobile protons (up to 13 M) using pH_2 and ammonium buffers at low-magnetic field. To accomplish this, polarization transfer routes from pH_2 to hydroxyl groups were first investigated using the standard IrCl(COD)(IMes) SABRE catalyst (**1a** in Fig. 1) activated by pyridine (Py) in deuterated methanol. Different ammonium buffers NH_4Cl, $(NH_4)_2CO_3$ and NH_4OH were used to increase the mobile proton concentration ($[^1H]$ in Table 1) and to chemically control the concentration of ammonia in solution by setting the pH using the equilibrium reactions 1 and 2 in the ESI.† By doing so, gradual ligand displacement of Py by ammonia bound to iridium could be forced as shown before by Vaneeckhaute *et al.*[23] This provided us with a varying set of conditions in which protic solvent hyperpolarization could be compared since pyridine and ammonia are known to impact the polarization of the labile protons.[9,18] The composition of samples **I–IV** and the labile protons concentrations are summarized in Tables S1 and S2 (ESI†) respectively. After bubbling pH_2 through the different SABRE solutions **I–IV** at mT fields, NMR spectra could then be obtained at 18.8 T using the Bruker field-cycling prototype described schematically in Fig. S1 and S2 (ESI†). By repeating the same polarization cycle but at varying low-magnetic field strengths between 0 and 20 mT, the polarization transfer field (PTF) profiles for the labile protons of the solvent (OH signal at 4.8 ppm) and for Py (*ortho*-proton signal at 8.5 ppm) could be constructed and are shown in Fig. 2. More details of the operating procedure and hardware specifications of the field-cycling setup can be found in the ESI,† Section 1.

First, the active SABRE catalyst in mixtures **I–IV** was characterized from analysis of the isolated proton region between $\delta = -20$ ppm and -25 ppm at 18.8 T. These signals correspond to the hydrides from the octahedral complexes in the general form of **2** in Fig. 1. Details of the catalytic activation of **1a** and the elucidation of the main catalytic species based on hyperpolarized 1D and 2D NMR of the hydride region can be found in the ESI,† Section 4 (Fig. S3–S5).[23] The following active SABRE octahedral complexes were found to be dominant and are summarized in Fig. 1: $[Ir(IMes)(H_2)(Py_{eq}Py_{eq}Py_{ax})]^+Cl^-$ (**2a**) for solution **I**, $[Ir(IMes)(H_2)(Py_{eq}N_{eq}Py_{ax})]^+Cl^-$ (**2b**) for solution **II**, $[Ir(IMes)(H_2)(Py_{eq}N_{eq}N_{ax})]^+Cl^-$ (**2c**) for solution **III** and $[Ir(IMes)(H_2)(N_{eq}N_{eq}N_{ax})]^+Cl^-$ (**2d**) for solution **IV**. An estimate of the relative abundance of each catalytic species considering the intensity of the hydride signals in the mixed-ligand complexes is given in Table S3 (ESI†).[24]

In Fig. 2a–c, the PTF analysis is shown for SABRE solution **I**, only containing pyridine as a ligand. The concentration of labile protons remains low at 0.08 M (Table 1) and the main catalytic complex present is complex **2a** in Fig. 1. The shape and maxima of the PTF profile contain insightful information on the polarization transfer routes and depend on the interplay between magnetic and chemical properties of the catalytic complex such as the *J*-coupling values between the hydrides mutually and between the targets, the chemical shift of the hydrides and the target protons, and the exchange rates of the targets on/off the transition metal.[25,26] Since these properties are target specific, in practice the PTF profiles can help us to trace the origin of the solvent hyperpolarization in the different SABRE solutions. For both the pyridine and solvent targets, the same maximum is noticed at 6 mT, a typical value where spontaneous polarization transfer from hydrides to aromatic target protons occurs.[27] Moreover, a strong correlation between the PTF profile of *ortho*-pyridine and the hydroxyl protons of methanol is apparent. This is shown in Fig. 2l (green) and hints towards polarization exchange occurring between pyridine and solvent molecules in agreement with observations made by Moreno *et al.*[18] The same is true when the solution was spiked with NH_4Cl in solution **II** and pyridine becomes partially displaced by ammonia from the iridium center (**2b** in Fig. 1).[23] Despite the change in the PTF profile of the pyridine protons in Fig. 2f (due to different stereochemistry and ligand

Table 1 Molar concentrations ($[^1H]$), molar polarization ($Px[^1H]$) and the longitudinal relaxation values (T_1) of the mobile solvent protons at 18.8 T of SABRE solutions **I–VI**. * For **I**, T_1 is considered an outlier. ** Negative polarization values indicate negative signal enhancements

Labile ^1H	I*	II	III**	IV	V	VI
$[^1H]$ (M)	0.08	0.48	0.88	1.73	6.68	13.28
$Px[^1H]$ (mM)	0.003	0.007	−0.065	−0.111	−1.79	−0.128
T_1 (s)	88.8 ± 61	26.6 ± 5.5	38.5 ± 2.0	33.2 ± 2.8	27.6 ± 7.8	17.3 ± 5.5

Open Access Article. Published on 29 October 2024. Downloaded on 12/19/2025 2:30:05 PM.
This article is licensed under a Creative Commons Attribution-NonCommercial 3.0 Unported Licence.

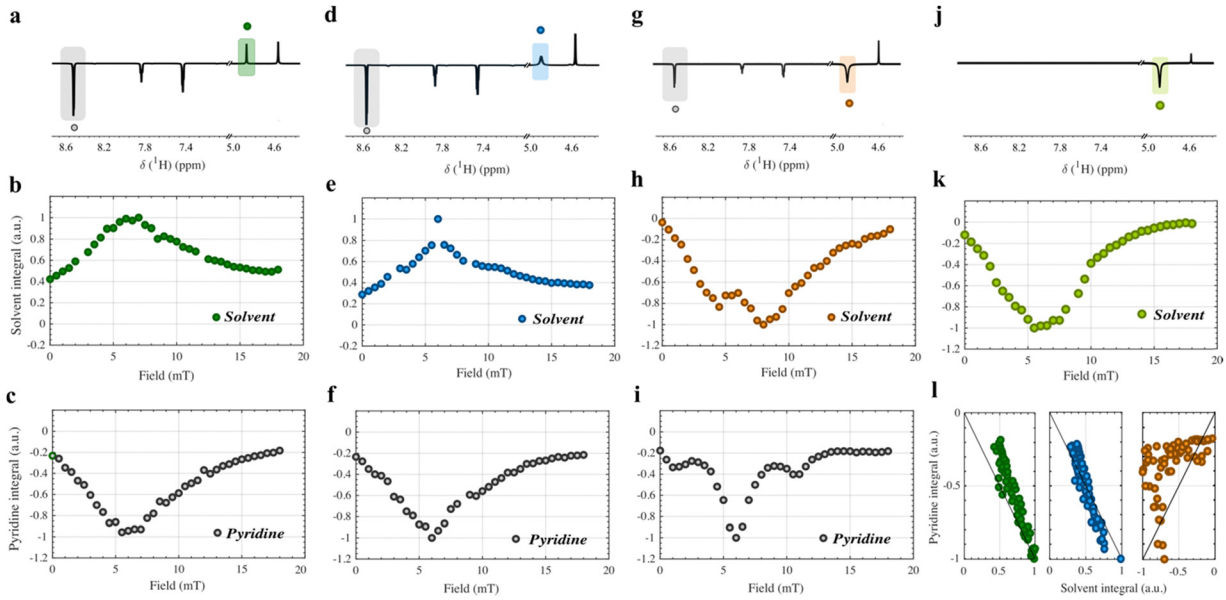

Fig. 2 Polarization transfer field (PTF) plots obtained for the hydroxyl signal (4.8 ppm) and the *ortho*-protons of pyridine (8.5 ppm) for SABRE solutions **I–IV**. The field-cycling prototype (Bruker) described in Fig. S1 and S2 (ESI†) was used to monitor the polarization induced at low-magnetic field between 0–20 mT after bubbling pH_2 through the SABRE solution. NMR signal integrals were then compared after detection at a field of 18.8 T. (a)–(c) PTF analysis of solution **I**. (d)–(f) PTF analysis of SABRE solution **II**. (g)–(i) PTF analysis of SABRE solution **III**. (j) and (k) PTF analysis of SABRE solution **IV**. (l) Correlation between the solvent hydroxyl NMR signal integral and the NMR signal integral of the *ortho*-proton of pyridine.

exchange properties[23]), it again mirrors the solvent PTF profile in Fig. 2e. The correlation plot is shown in Fig. 2l (blue). Intermolecular cross-relaxation between hydroxyl groups and the aromatic protons of pyridine at low-field is believed to be the mechanism for polarization exchange analogous to SPINOE.[12–14] In the fast tumbling regime, the polarization sign reverses due to more efficient double quantum cross-relaxation between dipolar coupled spins as can be seen here.[28] Other options such as direct polarization transfer to methanol binding to the catalyst using the lone electron pair on the oxygen are not considered important here.[21] First, the complex could not be detected by 1D and 2D NMR analysis of the hydrides (Fig. S3–S5, ESI†) most probably due to their short-lived nature.[29] Moreover, the expected difference in the exchange behavior of alcohols on transition metals, together with the different J-coupling network would impact the PTF profile of the solvent protons and would not lead to the correlated PTF profiles as observed here.[26] Even *ortho*-, *meta*- and *para*-protons of pyridine have different PTF profile shapes as shown in the ESI,† Section 5 (Fig. S6–S11). Thus, while hyperpolarization of labile solvent protons through cross-relaxation remains inefficient (between 0.003 and 0.007 mM, Table 1), it shows that SPINOE occurs and could be used as a general way to polarize molecules using hyperpolarized protic solvents.

When we further increased the dosage of both labile proton concentration and ammonia in SABRE mixtures **III** and **IV** (Table S1 and Section 3 in the ESI†), the hydroxyl solvent signal reversed sign as illustrated in Fig. 2g and j. Catalyst structure **2c** was most present for solution **III** and structure **2d** for solution **IV** as shown in Fig. 1 and Fig. S4 and S5 (ESI†). The polarization induced in the hydroxyl solvent protons (Fig. 2h) is not correlated anymore with the pyridine protons (Fig. 2i) as shown in Fig. 2l (orange). Instead, chemical exchange of hyperpolarized labile protons of ammonia starts to dominate and relays the negative polarization to the solvent analogous to the SABRE-RELAY method but under protic conditions.[9] More precisely the NHD_2 isotopologue[30] (Fig. S13, ESI†) ligated to iridium becomes hyperpolarized at low-field at an optimal field of around 6 mT. The low-field optimum for polarization of the solvent also lies at 6 mT and disregards the non-pairwise metathesis mechanism proposed by Emondts *et al.*[21] that shows maximum polarization transfer at 35 mT. Interestingly, the double maximum in the PTF profile solution **III** in Fig. 2h can be explained by the combined effect of chemical exchange induced polarization transfer and cross-relaxation induced polarization transfer to the solvent hydroxyl protons. The analysis is provided in Fig. S12 (ESI†). Overall, molar polarization levels rise to −0.1 mM for ammonium hydroxide (**IV**) even in the presence of 400 mM water (Table S1, ESI†).

Lastly, the potential for using ammonium hydroxide to hyperpolarize even larger concentrations of labile protons [^{1}H] in protic conditions was explored. [^{1}H] concentrations measured 6.68 M and 13.28 M in samples **V** and **VI** respectively, compared to 1.73 M labile protons present in sample **IV** (Table 1). Full sample compositions are summarized in Tables S4 and S5 (ESI†) (note that **VI** contains almost 10 mol% water). The thermal equilibrium and hyperpolarized solvent signals for samples **IV–VI** at 18.8 T are shown in Fig. 3. The hyperpolarized spectra were produced by bubbling pH_2 for 20 s at 6 mT. The integral of the thermal NMR signal rises proportionally to [^{1}H]. The linewidth at half height also rises with [^{1}H] from 7.5 Hz to 12.43 Hz and finally to 18.43 Hz. This is because radiation damping becomes significant at these high concentrations of protons.[31] The largest molar polarization of 1.79 mM was observed in sample **V**. A polarization of 0.025% was produced in 6.6 M of mobile protons. For all other

Open Access Article. Published on 29 October 2024. Downloaded on 12/19/2025 2:30:05 PM.
This article is licensed under a Creative Commons Attribution-NonCommercial 3.0 Unported Licence.

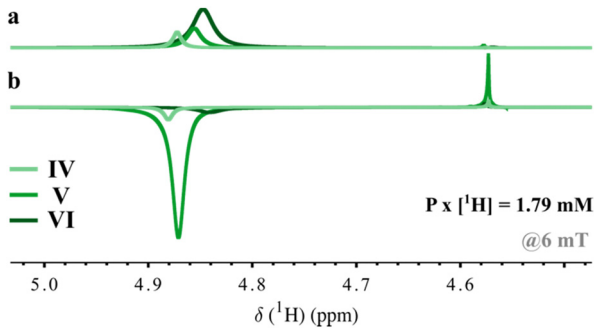

Fig. 3 Hyperpolarization of high concentrations of mobile protons (SABRE solutions **IV** to **VI**) using ammonium hydroxide in protic methanol/water (Table 1). (a) Thermal equilibrium signal (4.8–4.9 ppm) of solvent signal measured at 18.8 T. (b) Hyperpolarized negative solvent signal after field-cycling from 6 mT.

SABRE solutions, the molar solvent polarization produced at 6 mT can be found in Table 1 together with the corresponding characteristic relaxation time values (T_1) of the hyperpolarized labile protons measured at 18.8 T (Fig. S14, ESI†). For large mobile proton concentrations, T_1 decreased from 33 s with 1.73 M of mobile protons to 17 s with 13.28 M of mobile protons. The decrease in molar polarization generated for SABRE solution **VI** can be attributed to the decrease in lifetime of the hydroxyl protons, and the reduced solubility of hydrogen in water.

In conclusion, a molar polarization of up to 1.79 mM in mobile solvent protons of methanol/water mixtures was reached by introducing ammonium buffers at mT magnetic fields in the presence of the SABRE IrCl(COD)(IMes) catalyst and pH_2. Polarization transfer routes from pH_2 to the protic solvents were investigated by conducting field-cycling experiments to 18.8 T. Ammonia was found to fuel the solvent with negative polarization through chemical exchange of labile protons, while aromatic pyridine protons exchange polarization with the solvent *via* cross-relaxation and produce positive polarization instead. Hopefully, polarization exchange from the hyperpolarized protic solvent can be extended to other molecules and used as a general way to polarize molecules *via* pH_2.

This work was supported by the Hercules Foundation (AKUL/13/21) and by the Flemish Government, Department EWI *via* the Hermes Fund (AH.2016.134). E. V. acknowledges FWO-Vlaanderen for an FWO-SB fellowship and J. A. M. thanks the Flemish government for Methusalem support and acknowledges ERC for the ERC advanced grant WATUSO (No. 834134). NMRCoRe is supported by FWO Vlaanderen as International Research Infrastructure (I001321N).

Data availability

Hardware specifications, experimental methods, SABRE catalyst elucidation, PTF and lifetime analysis are provided in the ESI.† Raw NMR data and MATLAB scripts used for processing are available at **https://doi.org/10.5281/zenodo.13952093**.

Conflicts of interest

The authors declare no competing financial interest.

Notes and references

1 C. R. Bowers and D. P. Weitekamp, *J. Am. Chem. Soc.*, 1987, **109**, 5541–5542.
2 R. A. Green, R. W. Adams, S. B. Duckett, R. E. Mewis, D. C. Williamson and G. G. R. Green, *Prog. Nucl. Magn. Reson. Spectrosc.*, 2012, **67**, 1–48.
3 D. A. Barskiy, S. Knecht, A. V. Yurkovskaya and K. L. Ivanov, *Prog. Nucl. Magn. Reson. Spectrosc.*, 2019, **114–115**, 33–70.
4 R. W. Adams, J. A. Aguilar, K. D. Atkinson, M. J. Cowley, P. I. P. Elliott, S. B. Duckett, G. G. R. Green, I. G. Khazal, J. López-Serrano and D. C. Williamson, *Science*, 2009, **323**, 1708–1711.
5 J. Eills, D. Budker, S. Cavagnero, E. Y. Chekmenev, S. J. Elliott, S. Jannin, A. Lesage, J. Matysik, T. Meersmann, T. Prisner, J. A. Reimer, H. Yang and I. V. Koptyug, *Chem. Rev.*, 2023, **123**, 1417–1551.
6 F. Reineri, T. Boi and S. Aime, *Nat. Commun.*, 2015, **6**, 5858.
7 W. Iali, S. S. Roy, B. J. Tickner, F. Ahwal, A. J. Kennerley and S. B. Duckett, *Angew. Chem., Int. Ed.*, 2019, **58**, 10271–10275.
8 E. Vaneeckhaute, J.-M. Tyburn, J. G. Kempf, J. A. Martens and E. Breynaert, *Adv. Sci.*, 2023, **10**, 2207112.
9 W. Iali, P. J. Rayner and S. B. Duckett, *Adv. Sci.*, 2018, **4**, eaao6250.
10 K. Them, F. Ellermann, A. N. Pravdivtsev, O. G. Salnikov, I. V. Skovpin, I. V. Koptyug, R. Herges and J.-B. Hövener, *J. Am. Chem. Soc.*, 2021, **143**, 13694–13700.
11 E. T. Van Dyke, J. Eills, R. Picazo-Frutos, K. F. Sheberstov, Y. Hu, D. Budker and D. A. Barskiy, *Sci. Adv.*, 2022, **8**, eabp9242.
12 T. R. Eichhorn, A. J. Parker, F. Josten, C. Müller, J. Scheuer, J. M. Steiner, M. Gierse, J. Handwerker, M. Keim, S. Lucas, M. U. Qureshi, A. Marshall, A. Salhov, Y. Quan, J. Binder, K. D. Jahnke, P. Neumann, S. Knecht, J. W. Blanchard, M. B. Plenio, F. Jelezko, L. Emsley, C. C. Vassiliou, P. Hautle and I. Schwartz, *J. Am. Chem. Soc.*, 2022, **144**, 2511–2519.
13 O. G. Salnikov, I. A. Trofimov, A. N. Pravdivtsev, K. Them, J.-B. Hövener, E. Y. Chekmenev and I. V. Koptyug, *Anal. Chem.*, 2022, **94**, 15010–15017.
14 B. M. Goodson, *J. Magn. Reson.*, 2002, **155**, 157–216.
15 A. Sadet, C. Stavarache, M. Bacalum, M. Radu, G. Bodenhausen, D. Kurzbach and P. R. Vasos, *J. Am. Chem. Soc.*, 2019, **141**, 12448–12452.
16 J. H. Ardenkjær-Larsen, B. Fridlund, A. Gram, G. Hansson, L. Hansson, M. H. Lerche, R. Servin, M. Thaning and K. Golman, *Proc. Natl. Acad. Sci. U. S. A.*, 2003, **100**, 10158–10163.
17 E. Vaneeckhaute, J.-M. Tyburn, D. Kilgour, J. G. Kempf, F. Taulelle, J. A. Martens and E. Breynaert, *J. Phys. Chem. C*, 2020, **124**, 14541–14549.
18 K. X. Moreno, K. Nasr, M. Milne, A. D. Sherry and W. J. Goux, *J. Magn. Reson.*, 2015, **257**, 15–23.
19 S. Lehmkuhl, M. Emondts, L. Schubert, P. Spannring, J. Klankermayer, B. Blümich and P. P. M. Schleker, *ChemPhysChem*, 2017, **18**, 2426–2429.
20 E. W. Zhao, R. Maligal-Ganesh, Y. Du, T. Y. Zhao, J. Collins, T. Ma, L. Zhou, T.-W. Goh, W. Huang and C. R. Bowers, *Chem*, 2018, **4**, 1387–1403.
21 M. Emondts, D. Schikowski, J. Klankermayer and P. P. M. Schleker, *ChemPhysChem*, 2018, **19**, 2614–2620.
22 P. J. Rayner, B. J. Tickner, W. Iali, M. Fekete, A. D. Robinson and S. B. Duckett, *Chem. Sci.*, 2019, **10**, 7709–7717.
23 E. Vaneeckhaute, S. De Ridder, J.-M. Tyburn, J. G. Kempf, F. Taulelle, J. A. Martens and E. Breynaert, *ChemPhysChem*, 2021, **22**, 1170–1177.
24 L. Sellies, I. Reile, R. L. E. G. Aspers, M. C. Feiters, F. P. J. T. Rutjes and M. Tessari, *Chem. Commun.*, 2019, **55**, 7235–7238.
25 A. N. Pravdivtsev, A. V. Yurkovskaya, H.-M. Vieth, K. L. Ivanov and R. Kaptein, *ChemPhysChem*, 2013, **14**, 3327–3331.
26 S. Knecht, A. N. Pravdivtsev, J.-B. Hövener, A. V. Yurkovskaya and K. L. Ivanov, *RSC Adv.*, 2016, **6**, 24470–24477.
27 A. N. Pravdivtsev, K. L. Ivanov, A. V. Yurkovskaya, P. A. Petrov, H.-H. Limbach, R. Kaptein and H.-M. Vieth, *J. Magn. Reson.*, 2015, **261**, 73–82.
28 R. J. Fitzgerald, K. L. Sauer and W. Happer, *Chem. Phys. Lett.*, 1998, **284**, 87–92.
29 S. Knecht, S. Hadjiali, D. A. Barskiy, A. Pines, G. Sauer, A. S. Kiryutin, K. L. Ivanov, A. V. Yurkovskaya and G. Buntkowsky, *J. Phys. Chem. C*, 2019, **123**, 16288–16293.
30 E. Vaneeckhaute, J.-M. Tyburn, J. G. Kempf, J. A. Martens and E. Breynaert, *J. Phys. Chem. Lett.*, 2022, **13**, 3516–3522.
31 L. Dagys, M. C. Korzeczek, A. J. Parker, J. Eills, J. W. Blanchard, C. Bengs, M. H. Levitt, S. Knecht, I. Schwartz and M. B. Plenio, *Sci. Adv.*, 2024, **10**, eado0373.

 This journal is © The Royal Society of Chemistry 2024